J Mater Sci (2008) 43:4527–4533
DOI 10.1007/s10853-008-2644-8

Preparation of micro-spherical ZrO_2: Pr^{3+} phosphors by ultrasonic assisted CVS

Francisco Ramos-Brito · Manuel García-Hipólito · Castulo A. Alejo-Armenta · Enrique Camarillo · José M. Hernández · Héctor O. Murrieta · Ciro Falcony

Received: 24 October 2007 / Accepted: 9 April 2008 / Published online: 29 April 2008

Abstract Polycrystalline micro-spheres of undoped (ZO) and praseodymium-doped zirconia (PrZO) were obtained for different reactor temperatures (T_r) by the ultrasonic assisted chemical vapor synthesis process. SEM micrographs for $T_r \geq 400$ °C show that (a) the materials were synthesized in a powder form in the presence of particles spherical in shape with an average size of 3 μm and a narrow size distribution, and (b) the production of spherical particles had a remarkable increase on rate production and no considerable changes on their average size as T_r rises. EDS studies show an atomic percent composition of O-67.5, Zr-30.0, Pr-0.3, and Cl-2.2 for PrZO micro-spheres obtained at 500 °C, which is in good agreement with zirconium oxide stoichiometry. XRD patterns of ZO and PrZO micro-spheres for $T_r \geq 400$ °C show a polycrystalline tetragonal I structure with crystallite size values remaining below 20 nm. The photoluminescence emission spectrum of PrZO micro-spheres shows peaks overlapping the intrinsic emission of zirconia, attributed to inter-level transitions in Pr^{3+} ions: 490 and 505 nm: $^3P_0 - {}^3H_4$, 565 nm: $^3P_1 + {}^1I_6 - {}^3H_5$, 615 nm: $^1D_2 - {}^3H_4$ and 645 nm: $^3P_0 - {}^3H_6$. The excitation spectrum for the main emission peak (615 nm) shows that Pr^{3+} ions in PrZO show a preferred excitation through its 4f5d absorption band.

F. Ramos-Brito (✉) · C. A. Alejo-Armenta
Laboratorio de Materiales Optoelectrónicos, DIDe, Centro de Ciencias de Sinaloa, Av. De las Américas No. 2771 Nte. Col. Villa Universidad, Culiacan, Sinaloa C.P. 80010, Mexico
e-mail: rbrito@correo.ccs.net.mx; ramosbrito@fisica.unam.mx

M. García-Hipólito
Instituto de Investigaciones en Materiales de la Universidad Nacional Autónoma de México-UNAM, A.P. 70-360, Coyoacan 04510, DF, México

E. Camarillo · J. M. Hernández · H. O. Murrieta
Instituto de Física de la Universidad Nacional Autónoma de México-UNAM, A. P. 20-364 Del. A., Obregon 01000, DF, Mexico

C. Falcony
Departamento de Física, CINVESTAV-IPN, A.P. 14-740 G.A., Madero 07000, DF, Mexico

Introduction

Introduction of rare earth ions in metallic oxides commonly affects its wide energy band gap providing new optical properties or enhancing its intrinsic ones [1–4]. In the last decade, trivalent rare-earth doped metallic oxides have gained popularity like the most promissory luminescent materials [5]. Among advanced ceramic materials, zirconia (ZrO_2) plays an important role due to its chemical stability, photo-thermal stability, superior hardness, high refractive index, optical transparency, high thermal expansion coefficient, low thermal conductivity, ionic conductivity, polymorphic nature, and high thermo-mechanical resistance; it can be used in a variety of photonics applications [6].

The constant interest in developing inorganic phosphor materials with higher luminous efficiency, and providing the three basic colors needed in display parts as cathode ray tubes, field emission displays, and plasma displays panels [7], has led to the synthesis and study of rare-earth doped materials where the host materials used have a high-energy band gap, low phonon energy and chemical stability over photon and electron radiations [8]. In addition, phosphor particles must have a spherical morphology, small diameter, narrow size distribution, single phase, high purity, be non-aggregated, and compositionally uniform for good luminescent characteristics [8].

Phosphor powders, for full color display applications, need to emit light with wavelength values in three different basic colors: red (611–650 nm), green (510–580 nm), and blue (420–490 nm). Recently, studies on trivalent rare earth ions as luminescence activators in zirconia have been reported [9–13]. Emission spectra showed in these studies presented wavelength values, associated to emission peaks centered in the basic colors regions: 615 nm for praseodymium [9], 540, 614, and 619 nm for samarium [10, 13], 550 nm for erbium [12], 420, 546, and 617 nm for terbium [13], and 420 and 612 nm for europium-doped zirconia powders [13]. Even though these rare-earth doped zirconia powders present blue, green, and red emissions, its application in new flat panel displays demands another requirements as was mentioned above. The continuation of research activities on different synthesis routes or processes to obtain a phosphor with the required characteristics for its efficient incorporation in display technology could permit the improvement of its physical, chemical, and optical properties. This communication presents morphology, structural, chemical contents, and photo-luminescent studies on micro-spherical ZrO_2: Pr^{3+} phosphors obtained by ultrasonic assisted chemical vapor synthesis (UA-CVS) process at relatively low reactor temperature (T_r) values $\leq$500 °C, without any post-annealing treatments. This article complements other studies on doped zirconia previously reported by the same authors over the last few years [9, 14].

Experimental

Polycrystalline micro-spheres of undoped (ZO) and praseodymium-doped zirconia (PrZO) were obtained by the UA-CVS process. In this process, a solution with appropriate reactive materials is nebulized by an ultrasonic device and then carried by a filtered airflow through a pipe onto a heated substrate at atmospheric pressure where a pyrolysis reaction takes place. The reactor consists of a cubic container with liquid tin inside (at temperatures >300 °C), whose physical dimensions are 10 cm wide × 20 cm long × 5 cm high. The container has the upper face open and directly exposed to sprayed solution. The substrate works like a powder trap and it is laid on top of the liquid tin. The substrates were square pieces of pyrex glass with 1 × 1.5 cm dimensions. During the developed work, the synthesis of the powder was carried out varying different synthesis parameters: (a) doping concentration, (b) reactor temperature, (c) nozzle–substrate distance, (d) flow rate of the filtered air, and others. We reported just the results that we considered important; attending the characteristics of the resulting powders and their relevance to be employed in flat panel displays technology.

Several samples as a function of reactor temperature (T_r) were obtained. The precursor solution was prepared using zirconium oxichloride ($ZrOCl_2 + 8H_2O$, Aldrich Co.) and deionized water (resistivity 18 MΩ) at 0.05 M concentration. Praseodymium doping was achieved by adding $PrCl_3 + 6H_2O$ in a quantity of 1 at.% in relation to $ZrOCl_2 + 8H_2O$ content in this solution. T_r varied in a range from 300 to 500 °C. Ultrasonic generator frequency was 800 kHz. Flow rate of the filtered air was 8 L/min. The flow rate of the precursor solution was 1.5 mL/min. In all cases, for all reactor temperature values employed, the substrate temperature was 10 °C lower than what the reactor temperature indicated. The deposition time was 7 min in all cases. Micrographs to figure out the size and shape of the particles that form the powder, and their chemical composition by energy dispersive spectroscopy (EDS), were obtained, both with a Leica Cambridge Stereoscan 440 scanning electron microscope (SEM) equipped with a beryllium window X-ray detector. Prior to the EDS analysis, all the samples underwent a water desorption process to prevent interference on the chemical quantification by the water vapor absorbed in the samples. This procedure consisted of heating the sample at 200 °C and maintaining it at this temperature during 180 min. Every EDS reported result was obtained considering an average over three measurements collected from three different areas of 500 μm^2 each one. These areas were located in the center and two opposite edges of the substrate surface, were the powder particles were trapped. Crystalline structure was analyzed by grazing angle X-ray diffraction (XRD), using a Siemens D-5000 diffractometer with CuK_α radiation at 1.5426 Å. Identification of tetragonal phase and indexing of the peaks in the XRD patterns were done employing the equation $\sin^2\theta = A(h^2 + k^2) + Cl^2$, where $A(= \lambda^2/4a^2)$ and $C(= \lambda^2/4c^2)$ are constants for any one peak in the XRD pattern [15]. The crystallite sizes of the powders were obtained using Scherrer's formula: $t = (0.9\lambda)/(B \cos\theta_B)$ for peaks where 2θ was <35°. Room temperature photoluminescence excitation and emission spectra were recorded using a fluorescence spectrometer Perkin Elmer LS55.

The synthesis method was tested for reproducibility; in all cases, under the same parameter values, similar results were obtained.

Results and discussion

Even though studies on chemical composition, morphology, and crystalline structure as a function of doping concentration were done, we reported just the results that we considered important; attending the characteristics of the resulting powders and their relevance to be employed in flat panel displays technology, as we mentioned above.

In the present research we synthesized and characterized praseodymium doped zirconia (PrZO) samples from precursor solutions with $PrCl_3 \cdot 6H_2O$ contents in a range from 1 to 16 at.%, only results referent to PrZO obtained from a precursor solution with 1 at.% of $PrCl_3 \cdot 6H_2O$ are reported. The above mentioned was considered because there were not remarkable effects on the crystalline structure and morphology of light gray spheres (described in the article) with the doping concentration values employed here. In addition, EDS studies about chemical composition of light gray spheres as a function of doping concentration, and photoluminescent spectroscopy results, showed that PrZO obtained from a precursor solution with 1 at.% of $PrCl_3 \cdot 6H_2O$ present the major photoluminescence emission; this is in agreement with the results reported previously for PrZO powders obtained by co-precipitation technique [14]. In the rest of the article, the term PrZO will be associated to praseodymium-doped zirconia obtained from a precursor solution with 1 at.% of $PrCl_3 \cdot 6H_2O$.

Morphology

Polycrystalline micro-spheres of undoped zirconia (ZO) and PrZO were obtained by varying T_r parameter into the UA-CVS process. Figure 1 shows micrographs of ZO powders as a function of T_r. Micrographs obtained for PrZO powders as a function of T_r, not shown for the sake of brevity, are similar to those in Fig. 1. In both cases, samples obtained at $T_r \geq 400$ °C showed the synthesis of spherical-shaped particles with narrow size distribution and average size of 3 μm. The production rate of micro-spheres at low T_r values was poor and increased as T_r rised, this effect was associated with the insufficient thermal energy at low T_r values to complete evaporation of the majority of droplets; when T_r rises, the energy per droplet provided by the reactor starts to be enough to complete the particle growth mechanism. This mechanism includes droplet evaporation and transport of reactants, gas phase diffusion of the reactants, chemical reaction, particle growth,

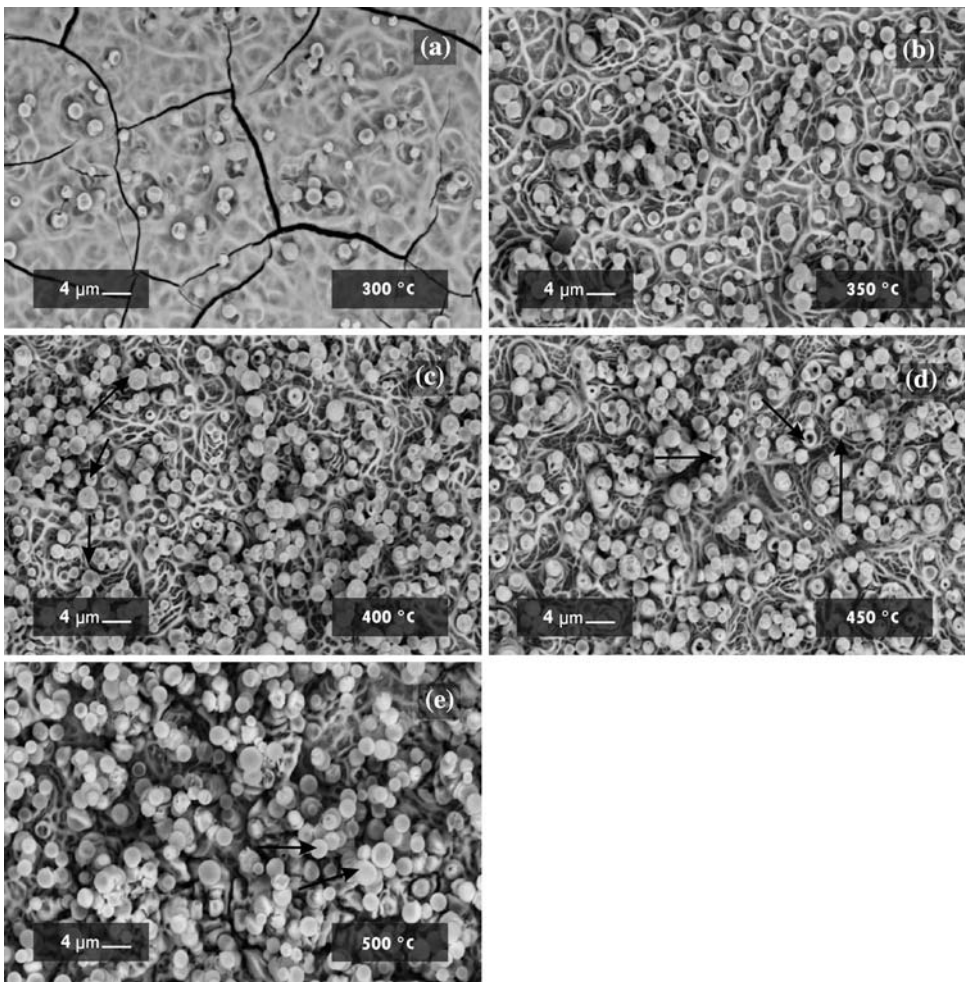

Fig. 1 Micrographs of ZO powders as a function of reactor temperature (T_r): (**a**) 300 °C, (**b**) 350 °C, (**c**) 400 °C, (**d**) 450 °C, and (**e**) 500 °C. Arrows in (**c**), (**d**), and (**e**) indicate dark gray, puffed, and light gray microspheres, respectively

structural arrangement, desorption of gas products, and deposition of the fine particles at the surface of the substrate [16]. At $T_r = 300$ °C, the majority of droplets sprayed on the substrate reach its surface, resulting in the deposition of a film with a high number of cracks and overall low quality, due to the poor synthesis of the final material on the substrate surface and desorption of the gas byproducts. At $T_r \geq 350$ °C, a 2-μm-thick film deposited on the substrate surface was observed. This film formation at the beginning of the process, without particle aggregation, was attributed to (a) the coexistence of film deposition and powder formation mechanisms during the process [17] and (b) the poor capacity of the substrate surface to trap micro-particles, due to the submicron roughness of the pyrex glass employed as substrate. After a short period of time that deposition started, the particles were trapped due to the roughness on the film initially formed on the substrate. Undoped and doped powders synthesized at T_r values in the range of 350–500 °C showed three kind of particles: (a) dark gray color particles, (b) puffed particles, and (c) light gray color particles; all three kinds showed surfaces with a certain degree of roughness, which decreases when T_r increases. This fact was associated to incomplete synthesis of the particles and slow desorption of gas byproducts at low T_r values, in agreement with the EDS results shown in Tables 1 and 2 for ZO and PrZO,

Table 1 Chemical element contents as a function of T_r for ZO powders

Reactor temperature T_r (°C)	Oxygen (at.%)	Zirconium (at.%)	Praseodymium (at.%)	Chlorine (at.%)
400	53.96	43.34	0	4.03
450	53.36	42.80	0	3.85
500	55.61	41.45	0	2.94

EDS results here reported are an average of measurements in three different areas of 500 μm^2 each one, located in the center, and two opposite edges of the substrate surface, where the powder particles were deposited

Table 2 Chemical element contents as a function of T_r for PrZO powders

Reactor temperature T_r (°C)	Oxygen (at.%)	Zirconium (at.%)	Praseodymium (at.%)	Chlorine (at.%)
300	67.91	25.42	0.08	6.62
350	53.57	39.37	0.33	6.73
400	52.74	41.86	0.28	5.12
450	52.57	42.87	0.36	4.20
500	52.06	44.81	0.47	2.66

EDS results here reported are an average of measurements in three different areas of 500 μm^2 each one, located in the center, and two opposite edges of the substrate surface, where the powder particles were deposited

Table 3 Elemental chemical composition for the three kinds of spherical particles observed in PrZO sample obtained at 450 °C

Sphere	Oxygen (at.%)	Zirconium (at.%)	Praseodymium (at.%)	Chlorine (at.%)
Light gray	67.52	29.93	0.33	2.23
Dark gray	24.86	67.18	0.73	7.23
Puffed	14.82	79.38	1.13	4.67

respectively. The types of particles mentioned above presented remarkable differences in their elemental contents as described below.

Chemical composition

Table 3 shows the chemical composition measurements for light gray, puffed, and dark gray spherical particles of PrZO obtained at 450 °C. Differences in elemental contents of the particles were observed, only the light gray color ones presented elemental contents in agreement with zirconia stoichiometry (ZrO_2). EDS measurements for puffed and dark gray color spheres showed an incomplete synthesis for these two types of particles, resulting in a zirconium oxide extremely rich in zirconium. EDS studies obtained for the three kinds of spheres of ZO obtained at 450 °C, but not shown for the sake of brevity, showed similar element contents of oxygen and zirconium to those observed for PrZO. In all EDS measurements, low values for data dispersion of element contents in the three different zones considered were observed, indicating a homogeneous distribution of the three types of spheres on the substrate surface. Table 1 shows the relative chemical element contents as a function of T_r for ZO powders. The element contents suggest that the powder material trapped on the substrate surface is a zirconium oxide rich in zirconium with traces of chlorine, but considering a surface covered by three types of micro-spheres (mentioned above) (see Fig. 1), the zirconium abundance and the remaining chlorine were attributed to the presence of puffed and dark gray color spheres on the surface, even at high T_r values. This result was in agreement with the XRD measurements presented in Fig. 2, where the presence of tetragonal phase of zirconia was confirmed and was attributed to the presence of the light gray spheres.

The changes on element contents experimented by ZO or PrZO powders when T_r rises were associated with the relative increase in the quantity of light gray spheres over the puffed and the dark gray color spheres, which is in agreement with the results obtained from Fig. 1. In order to justify this, an exercise that could be considered is to think that the elemental composition value of a given sample

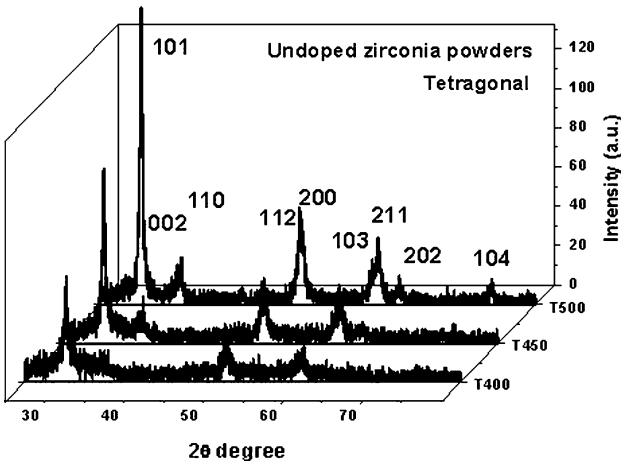

Fig. 2 Crystalline structure evolution as a function of reactor temperature (T_r) for ZO powders

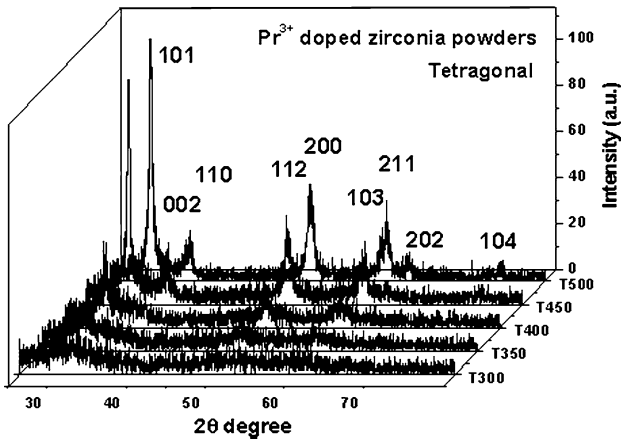

Fig. 3 Crystalline structure evolution as a function of reactor temperature (T_r) for PrZO powders

could be obtained by a lineal combination of the elemental composition for each type of particle, with integer coefficients determined by the number of each type of particle present in the sample, without considering the size distribution factor because there is a narrow distribution in this particular case. Then in this lineal equation it should be observed how the light gray coefficient increases over the dark gray and puffed coefficients, as T_r rises.

Table 2 shows the chemical composition of PrZO powders as a function of T_r. At $T_r = 300$ °C, the oxygen content is close to the element content required for zirconium oxide stoichiometry (ZrO_2), but the zirconium content was lower than expected; in addition, high chlorine content and extremely low powder production were observed too. This indicates the presence of precursor materials in the film and a low contribution of the powder in the element chemical quantification. In the case of powders synthesized at $T_r \geq 350$ °C, the changes on element contents as T_r rises were according with the relative increment on the rate production of light gray PrZO spheres, as in ZO powders happened. The decrease of chlorine content as T_r rises was associated with the increase of thermal energy per unitary volume and the consequent increase on the capacity to synthesize precursor materials; this is in agreement with the decrease observed of puffed and dark gray spheres on the surface as T_r increases.

Crystalline structure

Figures 2 and 3 show the crystalline structure evolution as T_r increases for ZO and PrZO powders, respectively. At low T_r values (<400 °C), ZO films and powders deposited on the substrate surface (see Fig. 1) are amorphous; this poor crystallization of zirconia is due to insufficient thermal energy for growth mechanisms of crystalline film and/or powder formation. These results are in agreement with the chemical composition determined by EDS results (see Tables 1 and 2). For T_r values ≥450 °C, a decrease on amorphous contribution and increase on intensities of the XRD peaks were observed. PrZO, on the other hand, presents XRD diffraction peaks even at low T_r. Both ZO and PrZO powders showed a well-defined tetragonal I crystalline phase for $T_r \geq 450$ °C. Tetragonal lattice parameters for ZO and PrZO powders, both obtained at 500 °C, were: $a = 3.60$ Å, $c = 5.16$ Å; and $a = 3.61$ Å, $c = 5.18$ Å, respectively. Tetragonal I phase of zirconia was associated to the crystal structure of the light gray color spheres, because (a) the increase on crystallinity coincides with the increase on production of light gray color spheres (see Fig. 1), (b) only the light gray color spheres showed element contents in good agreement with the ZrO_2 stoichiometry (see Table 3), and (c) the XRD measurements were performed by grazing angle X-ray diffraction, which reduces the substrate and base film contribution to XRD. Table 4 shows the crystallite size values as a

Table 4 Crystallite size values as a function of T_r for ZO and PrZO powders

Reactor temperature T_r (°C)	Crystallite size for undoped zirconia (nm)	Crystallite size for doped zirconia (nm)
300	[a]	2.57
350	[a]	6.53
400	15.23	12.85
450	18.28	19.13
500	19.13	17.88

Note: Scherrer formula, $t = (0.9\lambda)/(B \cos \theta_B)$, was employed to obtain crystallite sizes values

[a] XRD measurements were not indicating crystalline structure formation

function of T_r for ZO and PrZO powders. Crystallite size values, in the case of ZO, remained between 15.23 and 19.13 nm for T_r values in the range 400–500 °C. In the case of PrZO, even at 300 °C, it was possible to measure the crystallite size (2.57 nm). It is possible that Pr doping acts as a promoter of crystallite/particle formation. Due to the high homogeneity of starting precursor droplets and the consequent homogeneous gas phase diffusion of the reactants, crystallization occurred probably by homogeneous nucleation mechanism delaying the growth of crystallites resulting in overall small crystallite sizes <20 nm. This leads to lower surface energy and consequent stabilization of the tetragonal phase [18–20], without the presence of monoclinic phase previously reported for zirconia powders obtained by co-precipitation [14]. Similar characteristics between Pr^{3+} and Eu^{3+} ions (ionic radius: Pr = 1.09, Eu = 1.12; electronegativity: Pr = 1.1, Eu = 1.0) and studies of europium-doped zirconia reported by another authors [21] suggest the possible incorporation of Pr^{3+} ions in Zr^{4+} sites and the consequent creation of oxygen vacancies for charge compensation, promoting the stabilization of the tetragonal phase of zirconia. This is in agreement with the crystalline structure formation observed in praseodymium-doped zirconia at T_r = 300 and 350 °C (see Table 4).

Photoluminescence

Figure 4 shows the room temperature photoluminescent spectra of ZO and PrZO powders both obtained at T_r = 500 °C. The excitation wavelengths employed were 340 and 295 nm for ZO and PrZO, respectively. ZO powder showed its typical intrinsic white-blue luminescence, which consisted in a wide emission band centered at 490 nm starting at 400 and ending at 650 nm, in agreement with the previous results reported by other authors [10, 11]. Emission spectrum of praseodymium-doped zirconia showed five emission peaks overlapping the intrinsic emission of zirconia. The five peaks were attributed to inter-level transitions in Pr^{3+} ions, incorporated in the crystalline structure of zirconia, as follows: 490 and 505 nm to $^3P_0 - {}^3H_4$, 565 nm to $^3P_1 + {}^1I_6 - {}^3H_5$, 615 nm to $^1D_2 - {}^3H_4$ and 645 nm to $^3P_0 - {}^3H_6$, in agreement with the results previously reported for praseodymium in ziconia [14]. No changes in relative intensities of the emission peaks in PrZO spectrum as T_r increases were observed. The inset of Fig. 4 shows the intensity of the strongest emission peak (615 nm) in PrZO spectrum as a function of T_r. The highest emission intensity was observed for powders obtained at the highest T_r (500 °C). The increase in intensity of the 615 nm peak as T_r rises was associated to the increase in the quantity of light gray micron spheres on the substrate surface, and the consequent increase in crystallinity (see Figs. 1 and 3). These

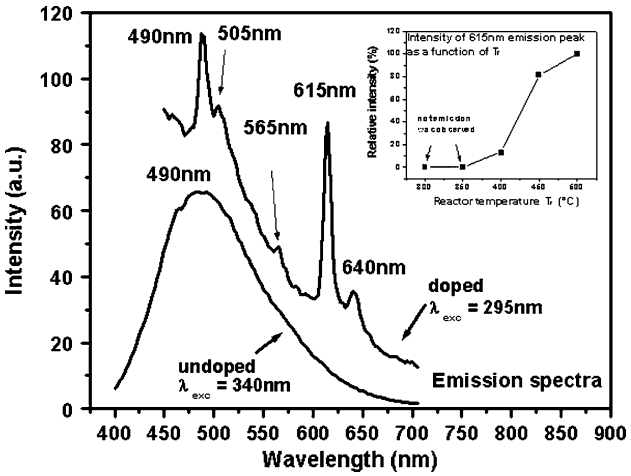

Fig. 4 Emission spectra of ZO and PrZO powders, with excitation wavelengths fixed at 340 and 295 nm, respectively. Powders of ZO and PrZO presented here were obtained at T_r = 500 °C

results suggested that the emission spectrum observed for PrZO powders was due to emission of light coming, mainly, from the praseodymium-doped tetragonal zirconia microspheres. Figure 5 shows the excitation spectra of ZO and PrZO powders both obtained at T_r = 500 °C. The emission wavelengths were fixed at 490 and 615 nm for ZO and PrZO, respectively. ZO spectrum showed two main excitation peaks centered at 280 and 340 nm, in agreement with the results reported previously [9]. PrZO excitation spectrum showed a main excitation peak centered at 295 nm associated to 4f5d praseodymium absorption band [9, 14] and another five excitation peaks with low intensity attributed to $^3H_4 - {}^3P_{j's}$ inter-level transitions in Pr^{3+} ions incorporated in the zirconia matrix [14]. This fact indicated a preference population of the $^1D_2$ energy level through 4f5d

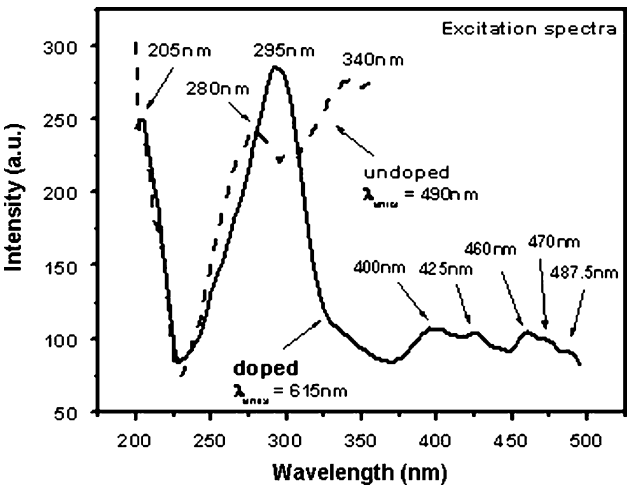

Fig. 5 Excitation spectra of ZO and PrZO powders, with emission wavelengths fixed at 490 and 615 nm, respectively. Powders of ZO and PrZO presented here were obtained at T_r = 500 °C

band over the direct excitation of $^3P_{j's}$ energy levels. Little asymmetry in 4f5d band due to overlapping of 4f5d praseodymium absorption band with 280 and 340 nm excitation band of zirconia was observed. Absorption starting at 220 nm to lower wavelength values was associated with transitions from band to band in zirconia (gap $\approx$ 5 eV).

Conclusions

Micro-spherical phosphors with red and white-blue color emissions, which present narrow size distribution and 3 μm average particle size, were obtained by UA-CVS at $T_r \leq 500$ °C without any post-annealing treatments. Spheres which emit in white-blue and red colors were constituted by undoped and praseodymium-doped tetragonal zirconia, respectively. A remarkable increase on particle production rate and no considerable changes on average size of these spherical particles were observed as T_r rises. Tetragonal I crystalline phase was the only phase observed for these zirconia white-blue and red phosphors. Lattice parameters for undoped and doped zirconia, both obtained at 500 °C, were: $a = 3.60$ Å, $c = 5.16$ Å; and $a = 3.61$ Å, $c = 5.18$ Å, respectively. No major changes on crystallite size values for samples obtained at $T_r \geq 400$°C were observed, remaining below 20 nm. White-blue and red color emissions were attributed to intrinsic zirconia emission centered at 490 nm and $^1D_2 - {}^3H_4$ electronic transition in Pr^{3+} ions incorporated in the crystalline structure of zirconia (wavelength of 615 nm), respectively. Red color emission from doped zirconia presented a preferred excitation through the 4f5d absorption band of praseodymium, centered in this case at 295 nm. White-blue color emission from undoped zirconia presented two main excitation wavelengths centered at 280 and 340 nm.

In the present research, the light-gray spheres were considered responsible for luminescence emission, where the emission intensity depends on (a) the quantity of light gray spheres on the substrate surface and (b) the praseodymium ion content in light gray spheres; this suggests that they maximize the light gray sphere production and minimize the production of the another two types of spheres in order to have a powder with better luminescence characteristics. The fact that our system employed here in this technique has a reactor temperature parameter limited to 600 °C invites to prove changes in another synthesis parameters. For example: could be considered the synthesis under same conditions but employing molarities lower than 0.05 M, which could optimize the energy/mass rate provided by the reactor, and should permit an increase of light gray spheres production over the puffed and dark gray spheres.

Acknowledgements The authors thank Leticia Baños, Daniel Brito-Ramírez, Lorena Uriarte, José Guzmán, Marcela Guerrero, Ana Soto, and Juan García Coronel for the technical support provided, and CECyT (Sinaloa-México) and CONACyT CB-2006-1-J1-I0002-57809 (México) for the financial grant for this investigation.

References

1. García-Hipólito M, Corona-Ocampo A, Álvarez-Fregoso O, Martínez E, Guzmán-Mendoza J, Falcony C (2004) Physica Status Solidi (A) 201:72. doi:10.1002/pssa.200306692
2. García-Hipólito M, Guzmán-Mendoza J, Martínez E, Álvarez-Fregoso O, Falcony C (2004) Physica Status Solidi (A) 201:1510. doi:10.1002/pssa.200306796
3. García-Hipólito M, Álvarez-Fregoso O, Guzmán J, Martínez E, Falcony C (2004) Physica Status Solidi (A) 201:R127. doi:10.1002/pssa.200409076
4. Martínez-Martínez R, García-Hipólito M, Ramos-Brito F, Hernández-Pozos JL, Caldiño U, Falcony C (2005) J Phys Condens Matter 17:3647. doi:10.1088/0953-8984/17/23/016
5. Blasse G, Grabmaier BC (1994) Luminescent materials. Springer, Berlin, pp 27–28, 40–50
6. Subbarao EC (1981) In: Heuer AH, Hobbs LW (eds) Advances in ceramics, vol 3. The American Ceramic Society Inc., Columbus, OH, pp 1–24
7. Yu M, Lin J, Fu J, Zhang HJ (2003) J Mater Chem 13:1413. doi:10.1039/b302600k
8. Mckittrick J, Shea LE, Bacalski CF, Bosze EJ (1999) Displays 19:169. doi:10.1016/S0141-9382(98)00046-8
9. Ramos-Brito F, García-Hipólito M, Martínez-Martínez R, Martínez-Sánchez E, Falcony C (2004) J Phys D: Appl Phys 37:L13. doi:10.1088/0022-3727/37/5/L01
10. De La Rosa-Cruz E, Díaz-Torres LA, Salas P, Rodríguez RA, Kumar GA, Meneses MA, Mosiño JF, Hernández JM, Barbosa-García O (2003) J Appl Phys 94:3509. doi:10.1063/1.1599960
11. Millers D, Grigorjeva L, Opalinska A, Lojkowski W (2003) Solid State Phenom 94:135
12. Friend CS, Patra A, Kapoor R, Prasad PN (2002) J Phys Chem B 106:1909. doi:10.1021/jp013576z
13. Reisfeld R, Zelner M, Patra A (2000) J Alloys Compd 300:147. doi:10.1016/S0925-8388(99)00714-8
14. Ramos-Brito F, Murrieta H, Hernández J, Camarillo E, García-Hipólito M, Martínez-Martínez R, Álvarez-Fragoso O, Falcony C (2006) J Phys D: Appl Phys 39:2079. doi:10.1088/0022-3727/39/10/016
15. Cullity BD, Stock SR (2001) Elements of X-ray diffraction, 3rd edn. Prentice Hall, New Jersey, pp 302–308
16. Messing GL, Zhang SC, Jayanthi GV (1993) J Am Ceram Soc 76:2707. doi:10.1111/j.1151-2916.1993.tb04007.x
17. Langlet M, Joubert JC (1993) In: Rao CNR (ed) Chemistry of advanced materials. Blackwell Science, Oxford, UK, p 55
18. Garvie RC (1965) J Phys Chem 69:1238. doi:10.1021/j100888a024
19. De Vicente FS, De Castro AC, De Souza MF, Siu Li M (2002) Thin Solid Films 418:222. doi:10.1016/S0040-6090(02)00784-8
20. Barnard AS, Yeredla RR, Xu H (2006) Nanotechnology 17:3039. doi:10.1088/0957-4484/17/12/038
21. Dexpert-Ghys J, Faucher M, Caro P (1984) J Solid State Chem 54:174. doi:10.1016/0022-4596(84)90145-2